Fluorescence signals of quantum dots influenced by spatially controlled array structures

2009 Nanotechnology 20 415201

(http://iopscience.iop.org/0957-4484/20/41/415201)

Nanotechnology **20** (2009) 415201 (5pp) doi:10.1088/0957-4484/20/41/415201

Fluorescence signals of quantum dots influenced by spatially controlled array structures

J W Chou[1], K C Lin[1], Y T Tang[1], F K Hsueh[2], Yao-Jen Lee[2], C W Luo[1], Y N Chen[3], C T Yuan[4], Hsun-Chuan Shih[1], W C Fan[1], M C Lin[5], W C Chou[1] and D S Chuu[1,6]

[1] Department of Electrophysics, National Chiao Tung University, Hsinchu 30050, Taiwan
[2] National Nano Device Laboratories, Hsinchu 30078, Taiwan
[3] Department of Physics, National Cheng Kung University, Tainan 701, Taiwan
[4] Research Center for Applied Sciences, Academia Sinica, Taipei 11529, Taiwan
[5] Department of Physics, Fu Jen Catholic University, Taipei County 24205, Taiwan

E-mail: dschuu@mail.nctu.edu.tw

Received 21 July 2009, in final form 20 August 2009
Published 16 September 2009
Online at stacks.iop.org/Nano/20/415201

Abstract
Fluorescence signals of quantum dots (QDs) influenced by different array structures of gold-coated silicon nanorods (SiNRs) were investigated via experimental observations and two-dimensional (2D) finite element method (FEM) simulations. On the densest gold-coated SiNRs array structure, the highest QD fluorescence quenching rates were observed and on the sparsest array structure, the highest QD fluorescence enhancement rates were observed. By developing a new technique which obtains the optical image of the array structures without losing information about the QD locations, we were able to further investigate how the QD fluorescence is influenced by spatially controlled array structures.

1. Introduction

The fluorescence emission from semiconductor nanoparticles can be significantly influenced by coupling with the localized surface plasmon (LSP) provided by metal surfaces [1–3]. By properly arranging the geometric configurations of a metal/dielectric interface, the properties of the LSP resonance modes, in particular, their interaction with light can be manipulated. For example, the topic of quantum dots (QDs) located within the range of surface plasmon polaritons [4–12] has been studied. Besides, many applications such as surface enhanced Raman scattering (SERS) [13–16], plasmon waveguides [17], filters and nanocavities [18], etc have been developed recently. In this paper, to investigate the coupling effects of QD fluorescence and the LSP resonance modes, we designed three different array structures, i.e. square periodic arrays of gold-coated silicon nanorods (SiNRs), for the experiments. The geometric size and shape of the Au-coated SiNRs in these three array structures are fixed; however, the distances between the Au-coated SiNRs are varied for spatial control of the LSP resonance modes. Both enhancement and quenching of the QD fluorescence influenced by the array structures were observed in the experiments. We further developed a new technique to define the relative locations between the QDs and the Au-coated SiNRs for observing how the relative locations influence the coupling effect. Finally, 2D finite element (FE) [19] simulations based on electromagnetic theory were applied for interpretations.

2. Experiment results and discussions

The descriptions of the three Au-coated SiNR arrays (scanning electron microscopy (SEM) images as shown in figures 1(A) (a)–(c)) used in our experiments can be found in our previous paper [20]. The commercially available core/shell (CdSeTe/ZnS) QDs [21] (diameter 5.3 nm, concentration $\sim 10^{-9}$ M) were spin-coated (∼5000 rpm) on a cover glass, and then each array structure was put upside down above the cover glass (the top of the Au-coated SiNWs was contacted with the QDs on the cover glass) as shown in figure 1(B).

[6] Author to whom any correspondence should be addressed.

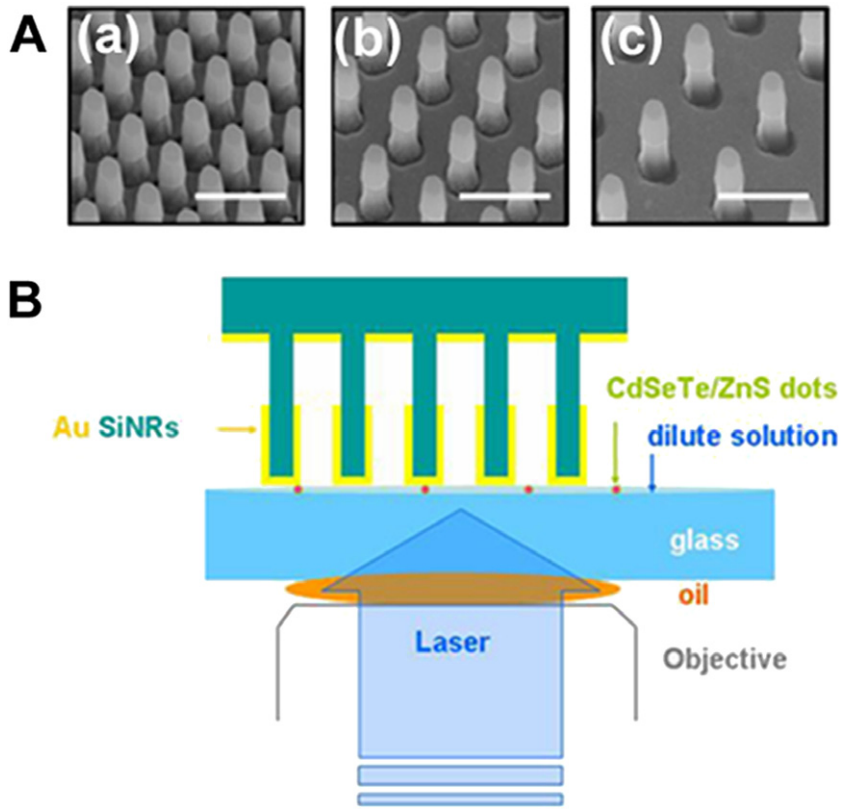

Figure 1. (A) ((a)–(c)) SEM images of Au-coated SiNRs arrays [a–c]. Scalar bars shown in (a)–(c) are 1 μm. (B) Schematic view of the sample structure.

(This figure is in colour only in the electronic version)

QDs fluorescence signals were measured by a PicoQuant Microtime200 confocal microscope system (with the objective: Olympus UPlanSApo 100xoil, NA = 1.4). The picosecond pulsed diode laser (repetition frequency: 10 MHz, wavelength 405 nm, power $\sim$ 0.02 μW) was used as the excitation source for obtaining sufficient statistical lifetime histograms, and a long pass 500 nm filter was used to filter out the excitation laser. The fluorescence images (areas: 4.75 $\times$ 4.75 μm^2) of the 50 different QDs on arrays [a–c] and on the glass are shown respectively in figures 2(A) (a)–(d). In figure 2(B), total event number distribution statistics of enhancement factors from the 50 different QDs of arrays [a–c] (the black, red, and green columns are for the QDs on arrays [a–c]) are shown. The enhancement factor was calculated by the intensity value on arrays [a–c] divided by the intensity value on the glass, respectively. The intensity value can be obtained from the integration of the multi-channel scalar (MCS) trace/the record time. One of a segment of MCS trace is shown in figure 2(C) (a). The statistical quenching (enhancement) rate is defined as the rate of the quenching (enhancement) event numbers/total event numbers. The quenching rates ($Q\%$) and enhancement rates ($E\%$) were obtained from the target 50 QDs (classified by the enhancement factor). Since the error bar of the fluorescence intensity of the same point (obtained from the average of ten measurements) of QDs is $\sim$5%. Therefore, we assume that when the intensity variation of the QD fluorescence $>$10%, the extra variation is due to the phenomena of quenching or enhancement. For each point of QDs, the enhancement factor $<$0.9 is classified as quenching, whereas the enhancement factor $>$1.1 is classified as enhancement. For the 50 different QDs on arrays [a–c], the quenching rates are $\sim$46%, 10%, and 8% respectively, and the enhancement rates are $\sim$42%, 74%, and 82% respectively. We find that among the three array structures, the QDs fluorescence on array [a] exhibits the highest quenching rate, whereas that on array [c] exhibits the highest enhancement rate. According to the results of the reflectance spectra of three different array structures in our previous paper [20], the LSP mode of array [c] is close to the fluorescence wavelength 705 nm [20]. The highest coupling efficiency is reached when the LSP resonance is formed [10]. In our case, the sparsest array structure provides such LSP resonance frequency coincidentally, which is a key point indicating that among the three array structures, array [c] provides higher coupling efficiency for QD fluorescence enhancement. In other words, QD fluorescence on array [c] can be efficiently enhanced due to it being the sparsest array structure where the localized surface plasmon resonance forms.

In figures 2(C) (a) and (b), the multi-channel scalar (MCS) trace and the time-correlated single photon counting (TCSPC) histogram of one of the single quantum dots (SQDs) picked up from the 50 QDs on arrays [a–c] and on the glass are shown respectively. The MCS trace reveals the SQD fluorescence intensity fluctuation in $\sim$15 s, and the TCSPC histogram reveals the SQD fluorescence lifetime statistics

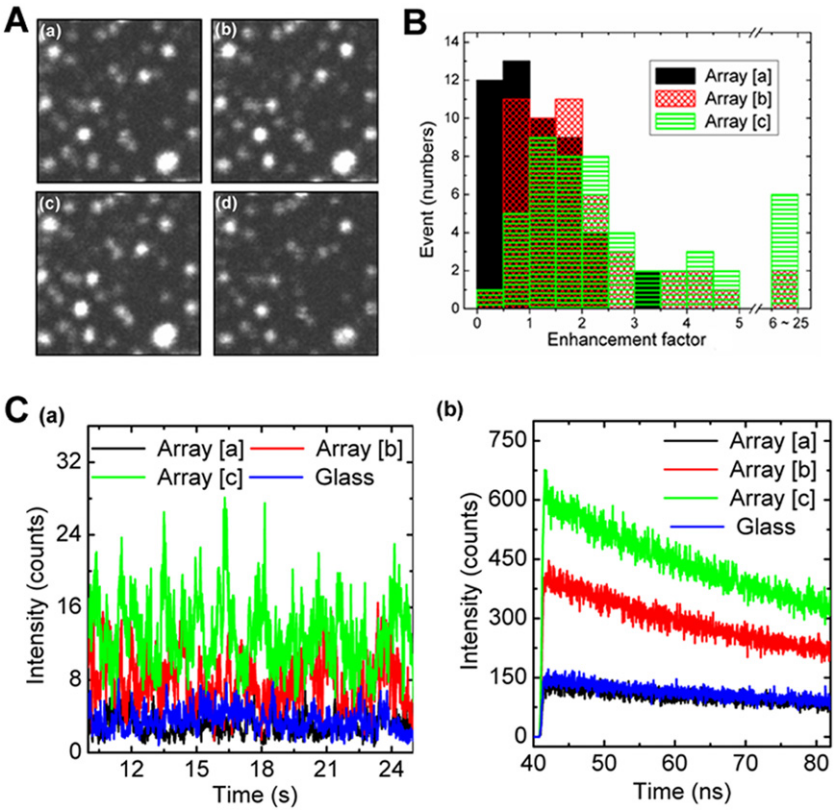

Figure 2. (A) ((a)–(d)) Fluorescence images of 50 different QDs on arrays [a–c] are shown in (a)–(c) and that on the glass is shown in (d). The fluorescence image areas are $4.75 \times 4.75\ \mu m^2$. (B) Statistic event numbers of the enhancement factors are taken from 50 different QDs of arrays [a–c]. Array [a] shows the highest quenching rate; while array [c] shows the highest enhancement rate. (C) (a) the MCS and (b) the TCSPC of one of the SQD picked up from the 50 QDs on arrays ([a–c]) and on the glass.

(recording time: 1 min). According to TCSPC histograms, the fluorescence intensities of SQD on arrays [a–c] and on the glass can be fitted by single exponential decay: $I = A_0 + A_1 e^{-t/\tau_1}$. In the case as shown in figure 2(C), the SQD is not close to the Au-coated SiNRs on arrays [a–c], so that the quenching effects are avoided. The enhancement factors of the SQD on arrays [a–c] are 0.91, 2.40 and 3.63, and the lifetimes (τ_1) are 50.12 ns, 47.90 ns, and 49.57 ns respectively.

We further investigated the influence of the relative locations between the SQD and the Au-coated SiNR of array [c] as shown in figures 3(A)–(C). In figure 3(A) (a), six different relative locations (p1–p3, d1–d2, x) of the same SQD fluorescence image are shown. The six SQD fluorescence image areas shown in figure 3(A) (a) are $3 \times 3\ \mu m^2$. In order to define the relative locations between the SQD and the Au-coated SiNR, we removed the long pass 500 nm filter, and focused the laser light near each array substrate. Therefore, the substrate regions are bright and the Au-coated SiNRs regions are dark, such that the array structures are distinguishable. The stability of the system was carefully checked by comparing the drift distances (<2.5 nm in 1 min) of the SQD locations before and after measuring the reflection images. Array [c] was selected for the experiment since its optical reflectance image is the most obvious one. One of the reflectance images for defining the relative locations as shown in figure 3(A) (b) of array [c] was formed by scanning the same area with the fluorescence images as shown in figure 3(A) (a). Then, a schematic array with the peripheral (green short dash lines) and the diagonal (olive long dash lines) direction assisting lines for the following descriptions was additionally sketched. Fluorescence intensity of the same SQD was observed by randomly replacing array [c] on different relative locations. In figure 3(A) (b), six typical relative locations with color points labeled for the p1–p3 (for the peripheral directions), d1–d2, and x (for the diagonal directions) of the same SQD are shown. The MCS trace shown in the inset of figure 3(B) (a) reveals the SQD fluorescence intensity fluctuation in ∼5 s, and the TCSPC and the normalized TCSPC histograms in figures 3(B) (a) and (b) reveal the SQD fluorescence lifetime statistics (recording time: 1 min). In figures 3(B) (a) and (b), the MCS traces and the TCSPC of the SQD on location x, d1–d2, p1–p3 on array [c] are shown. According to TCSPC histograms, the fluorescence intensities of a SQD on array [c] also can be fitted by single exponential decay. The lifetimes (τ_1) of SQD on x, d1–d2, p1–p3 are 53.4 ns, 47.9 ns, 42.6 ns, 40.1 ns, 28.7 ns, and 22.5 ns respectively. The corresponding enhancement factors on each one are 0.8, 2.0, 2.5, 2.7, 3.3, and 4.4. The higher enhancement factors are attributed to two reasons, the LSP coupling and the constructive interference. First of all, the LSP coupling process occurs as the SQD is located close to the boundary of the Au-coated SiNR, e.g. locations d2 and p2–p3. Second, the SQD fluorescence is enhanced when SQD

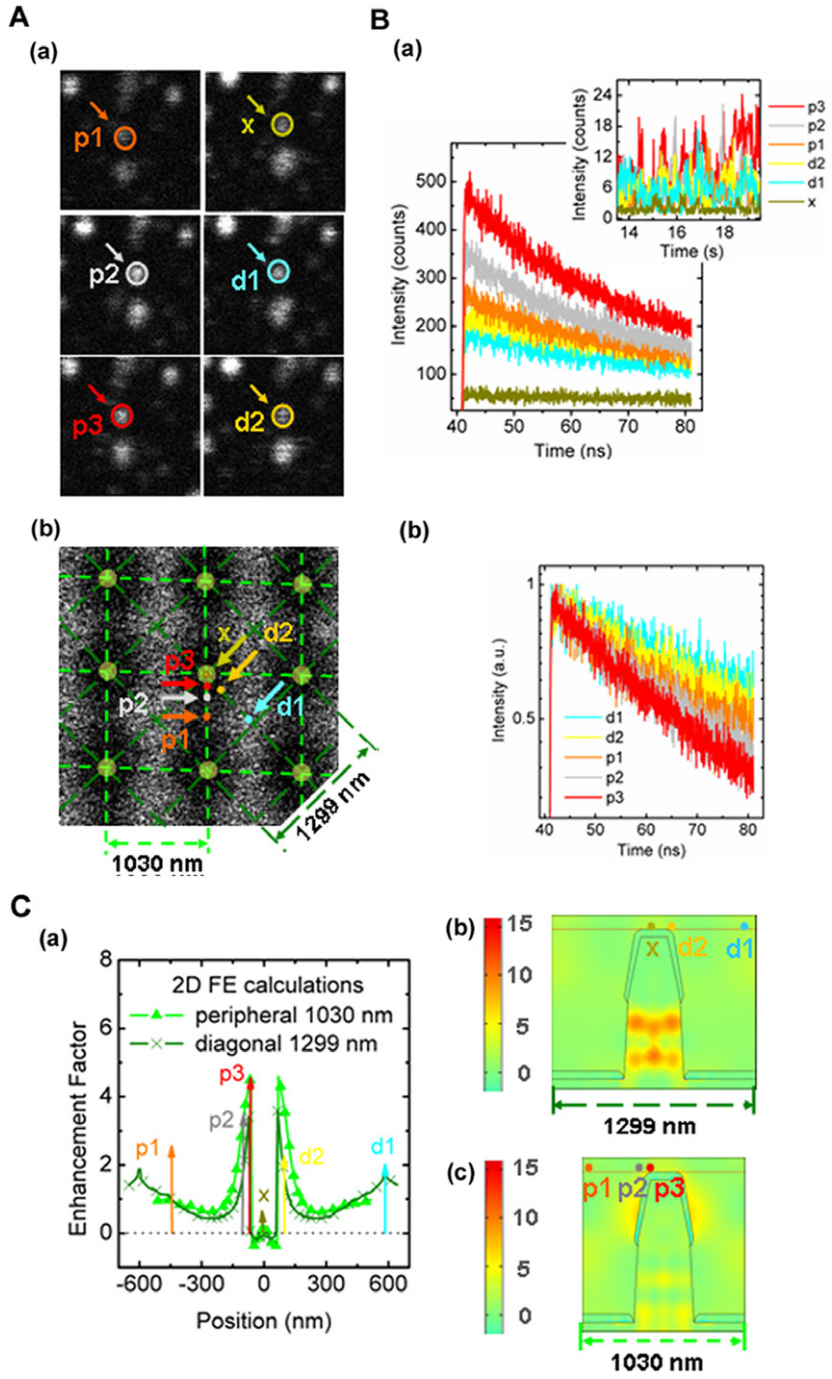

Figure 3. (A) (a) The QD fluorescence images for six different relative locations (labeled as p1–p3, d1–d2, x). The images areas are 3×3 μm^2. (b) The reflectance image combined with the schematic square unit cell of array [c] and color points labeled for six different locations (p1–p3 (the peripheral direction), d1–d2 (the diagonal direction), x (the center of Au-coated SiNR)) of the same SQD are shown. (B) (a) TCSPC and MCS trace (the inset). (b) Normalized log scale TCSPC of the SQD on locations x, d1–d2, p1–p3 of array [c] (dark yellow, blue, yellow, orange, gray, and red line). (C) ((a)–(c)) 2D FE calculations of the unit cell of array [c] are shown (color labels x, d1–d2, p1–p3 from the experiments are listed for comparison). (a) 'Position versus enhancement factors' on the 0 nm line above Au-coated SiNR. The normalized time average total energy densities in the diagonal direction (the olive line) and the peripheral direction (the green line) of the unit cell are shown in (b) and (c) respectively. The color codes for (b) and (c) are the absolute values of the time average total energy densities normalized to the incident total energy densities.

is located near the mid-point of two Au-coated SiNRs where the constructive interference is formed, e.g. locations d1 and p1. However, when the SQD touches the Au-coated SiNR, e.g. location x, the enhancement factor is decreased due to the dissipation process.

In figures 3(C) (a)–(c), we used the FEM [19] simulations as implemented in the FEMLAB code (www.femlab.de) to calculate the time average total energy densities on a unit cell of array [c] for comparison with the experiment results. The simulation details can be found in our previous papers [12, 20].

The Helmholtz wave equation was solved within a unit cell by employing periodic boundary conditions for each case, and the TM mode plane wave based calculations corresponding to the LSP resonance were obtained. In figure 3(C) (a), 'the enhancement factors versus the position' on the 0 nm line above the Au-coated SiNRs are shown for both the peripheral (green line) and the diagonal (olive line) direction on array [c]. Consistent with the experimental results, we find that on the center regions of the 0 nm line above the Au-coated SiNR (location x), the enhancement factor is about 0 which corresponds to the quenching effect, whereas on the boundary regions (locations d2 and p2–3) of the Au-coated SiNR and the constructive interference regions (locations d1, p1), the enhancement factors are higher. The time average total energy densities on a unit cell of array [c] at incident wavelength 705 nm in the diagonal and peripheral direction are shown in figures 3(C) (b) and (c) respectively.

3. Conclusion

In conclusion, we found that QD fluorescence on the sparsest array structure shows the highest enhancement rate due to the highest coupling efficiency with the radiative LSP resonance frequency; whereas QD fluorescence on the densest array structure shows the highest quenching rate due to the largest contact areas with the Au-coated SiNRs, which provide the largest regions for the fluorescence dissipation. Further, from the observations with the identified relative locations between the QDs and the array structures, we found that the QD fluorescence enhancement effects are observed on the locations close enough to the Au-coated SiNRs (but not touching the Au) and on the locations near the mid-point of two Au-coated SiNRs. Finally, 2D FEM simulation results are consistent with the experimental results. The array structures we studied were fabricated by well-established silicon technology and are reproducible. By implementing careful design, more efficient composite optical devices could be fabricated.

Acknowledgments

One of the authors (J W Chou) sincerely thanks Yan-Cheng Lin, Hui-Lin Chung, Wei-Jhih Wang at the Department of Electrophysics, NCTU, and Yun Wan, Ruei-Fu Jao at the Department of Physics, Fu Jen Catholic University, Taiwan, and M Becker, S H Christiansen, and U Goesele at Max Planck Institute of Microstructure Physics, Halle, Germany for experimental support and valuable discussions. This work is supported partially by the National Science Council, Taiwan, under grant no. NSC 97-2112-M009-004.

References

[1] Ritchie R H 1957 *Phys. Rev.* **106** 874–81
[2] Stern E A and Ferrell R A 1960 *Phys. Rev.* **120** 130–6
[3] Barnes W L, Dereux A and Ebbesen T W 2003 *Nature* **424** 824–30
[4] Gueroui Z and Libchaber A 2004 *Phys. Rev. Lett.* **93** 166108
[5] Pons T, Medintz I L, Sapsford K E, Higashiya S, Grimes A F, English D S and Mattoussi H 2007 *Nano Lett.* **7** 3157–64
[6] Larkin I, Stockman M, Achermann M and Klimov V 2004 *Phys. Rev.* B **69** 121403
[7] Gryczynski I, Malicka J, Jiang W, Fischer H, Chan W, Gryczynski Z, Grudzinski W and Lakowicz J 2005 *J. Phys. Chem.* B **109** 1088–93
[8] Wang Y, Yang T, Tuominen M T and Achermann M 2009 *Phys. Rev. Lett.* **102** 163001
[9] Kulakovich O, Strekal N, Yaroshevich A, Maskevich S, Gaponenko S, Nabiev I, Woggon U and Artemyev M 2002 *Nano Lett.* **2** 1449–52
[10] Song J-H, Atay T, Shi S, Urabe H and Nurmikko A V 2005 *Nano Lett.* **5** 1557–61
[11] Chang D E, Sørensen A S, Hemmer P R and Lukin M D 2006 *Phys. Rev. Lett.* **97** 053002
[12] Christiansen S H, Chou J W, Becker M, Sivakov V, Ehrhold K, Berger A, Chou W C, Chuu D S and Gösele U 2009 *Nanotechnology* **20** 165301
[13] Fe'lidj N, Aubard J, Le'vi G, Krenn J R, Salerno M, Schider G, Lamprecht B, Leitner A and Aussenegg F R 2002 *Phys. Rev.* B **66** 233202
[14] lbach H and Lüth H 2002 *Solid-State Physics—An Introduction to Principles of Materials Science* 2nd edn (Berlin: Springer)
[15] Christiansen S H, Becker M, Fahlbusch S, Michler J, Sivakov V, Andrae G and Geiger R 2007 *Nanotechnology* **18** 035503
[16] Becker M, Sivakov V, Goesele U, Stelzner T, Andra G, Reich H J, Hoffmann S, Michler J and Christiansen S H 2008 *Small* **4** 398–404
[17] Maier S A, Kik P G, Atwater H A, Meltzer S, Harel E, Koel B E and Requicha A G 2009 *Nat. Mater.* **2** 229
[18] Bozhevolnyi S I, Smolyaninov I I and Zayats A V 1995 *Phys. Rev.* B **51** 17916
[19] Jin J 2002 *The Finite Element Method in Electromagnetics* 2nd edn (New York: Wiley)
[20] Chou J W *et al* 2009 *Nanotechnology* **20** 305202
[21] http://tools.invitrogen.com